FULL PAPER

Rapid Synthesis of Near Infrared Polymeric Micelles for Real-Time Sentinel Lymph Node Imaging

Dipanjan Pan, Xin Cai, Benjamin Kim, Allen J. Stacy, Lihong V. Wang,* and Gregory M. Lanza*

In this manuscript a synthetic methodology for developing sub 20 nm sized polymeric micellar nanoparticles designed for extravascular imaging and therapy is revealed. A simple, one-pot method is followed, which involves a rapid co-self-assembly of an amphiphilic diblock copolymer (PS-*b*-PAA) and polyoxyethylene (80) sorbitan monooleate in water. Sorbitan monooleate imparts stability to the micelles and helps to drive down the particle size below 20 nm. The particles are incorporated with a water soluble dye ADS832WS, which absorbs in the near infrared range (λ_{ex} = 832 nm) for sensitive detection with optical and photoacoustic imaging techniques. A candidate lipophilic anti-angiogenic therapeutic agent fumagillin was also incorporated with high entrapment (>95%) efficiency. The effectiveness of this theranostic platform for real-time, high-resolution intraoperative photoacoustic imaging for facilitating direct assessment of the sentinel lymph nodes (SLN) in breast cancer staging is demonstrated. The technique offers huge potential providing faster resection of SLN and may minimize complications caused by axillary exploration due to mismarking with dyes or low-resolution imaging techniques. Finally, the biodistribution and organ accumulation of the intravenously and intradermally injected particles are studied in a rodent model by optical imaging. Data suggest that intraveneously injected NIR-polymeric nanoparticles follow a typical bio-distribution clearance path through the reticuloendothelial (RES) system. For the intradermally injected particles, a slower mechanism of clearance is noticed.

1. Introduction

The use of mammography in women has increased the detection of small tumors with fewer involved axillary lymph nodes. While advances in all medical imaging modalities have been shown to identify suspicious nodes, their incidence of false-negative findings as well as their failure to detect small metastases have forced a reliance on microscopic examination at the time of axillary lymph node dissection (ALND).[1,2] The importance of accurate lymph node assessment is not only essential for disease staging and prognosis, but also fundamental for treatment planning decisions. Since breast cancer spreads to one or a few lymph nodes, the sentinel lymph node(s) (SLNs), before further metastasing to other axillary nodes, the identification and sampling of SLN, known as sentinel node biopsy (SNB), has successfully reduced the need for ALND and reduced the associated morbidity.[3–8] Consequently, SLB has become widely practiced in the United States, Europe, and Australia.

SLB requires noninvasive detection of SLN, which are marked for intraoperative localization and resection with methylene blue dye or radioactive colloid placed preoperatively under imaging guidance. SLN dye staining is approximately 90% effective, which can be improved to over 95% with radioactive colloid labeling but with added expense and inconvenience of intraoperative gamma camera imaging. The most sensitive approach involves radioactive colloids, which beyond the safety and handling issues surrounding radioactive materials in the operating room, the strong signal provides very low lateral and neglible vertical resolution to guide the resection, leading to imprecision in the localization and resection of SLN and increasing the potential for adverse surgical effects. For the methylene blue approach, there is no intraoperative image guidance and the location and depth of dissection must be approximated from pre-operative data. Moreover, allergic reactions to the blue dye are the most significant adverse event associated with the SLB.[9] Unfortunately, identification of the dye in the operating room can be hampered by changes in SLN orientation relative to external landmarks due to patient repositioning at surgery. Real-time high-resolution intraoperative imaging using a flexible, portable non-nuclear modality could facilitate direct assessment of the SLN location within the axilla independent of the patient position on the OR table. With immediate imaging, the resection of SLN would be faster and minimize complications

Prof. D. Pan, B. Kim, A. J. Stacy, Prof. G. M. Lanza
C-TRAIN and Division of Cardiology
Washington University School of Medicine
4320 Forest Park Avenue
Saint Louis, Missouri 63108, USA
E-mail: dipanjan@wustl.edu (Polymer)
X. Cai, Prof. L. V. Wang
Department of Biomedical Engineering
One Brookings Drive
Washington University
St. Louis MO
E-mail: lhwang@biomed.wustl.edu (Photoacoustics)

DOI: 10.1002/adhm.201200087

caused by axillary exploration due to mismarking with dyes or low resolution imaging techniques.

Photoacoustic (PA) or optoacoustic imaging is a non-invasive technique that uniquely synergizes optical and ultrasound imaging, providing high spatial resolution imaging in both the vertical and lateral planes.[10,11] The technique is based on a phenomenon in which the absorbed electromagnetic energy of light is transformed into kinetic energy and localized heating releasing a pressure or radiofrequency wave. The optical absorption can be associated with endogenous molecules, such as hemoglobin or melanin, or it can be achieved through exogenously delivered contrast agents: e.g. optical dyes, gold nanoparticles, single walled carbon nanotube (SWNT).[12–14] Recently, we[15] and other groups[16] have recently shown the utility of gold nanoparticles (≤90 nm) for preoperatively enhancing SLN detection. However, the clinical use of gold is discouraged by the high and unpredicatable cost of the metal; moreover, the added patient inconvenience, healthcare cost, and small risks involved with preoperative labeling persist.

We hypothesized that PA nanoparticle size and composition would dictate work the lymphatic transport behaviour based on prior work with gold nanoparticles. In addition, we anticipated that sub 20 nm "soft" polymeric nanoparticles, which are essentially the same size as small proteins, such as albumins, would have the most rapid lymphatic transit times yet be large enough for retention and phagocytosis by draining cortical macrophages. Polymeric nanoparticle at a size range of 15–20 nm would be highly advantageous over other previously used nanoplatforms in terms of their safety and facile lymphatic transport. Since these particles are meant to traverse rapidly through the lymphatic vessels, they can be tracked real-time and may assist direct evaluation of the SLN location. With the help of real time imaging, the resection of SLN would be quicker reducing the possibility of post-operative complications.

Polymeric nanoparticles can be produced in a variety of sizes and shapes.[17–19] In an early report, stable nanoparticles (30–40 nm) of polystyrene-*b*-poly(acrylic acid) (PS-*b*-PAA) copolymers were produced with increased hydrophobic core density though a high temperature annealing process.[20] Subsequently, similarly sized particles (~40 nm) targeted to folate, $\alpha_v\beta_3$-integrin, and or labeled with ^{64}Cu, were reported.[21–23] More complicated core-shell-corona micelles with a thermoresponsive shell self-assembled by triblock copolymer of poly(ethyleneglycol)-*b*-poly(N-isopropylacrylamide)-b-polystyrene (PEG_{45}-*b*-$PNIPAM1_{68}$-b-PS_{46}) (~40 nm) incorporating poly(N-isopropylacrylamide for thermo-sensitivity were described, to enhance localized drug delivery.[24] These agents, if targeted to caveolae for extravascular imaging or drug delivery will encounter significant size-dependent inefficiency. The objective of the present study was to develop a stable PS-*b*-PAA nano system with a sub 20 nm particle size with broad biomedical potential for extravascular imaging and drug delivery *in vivo*.

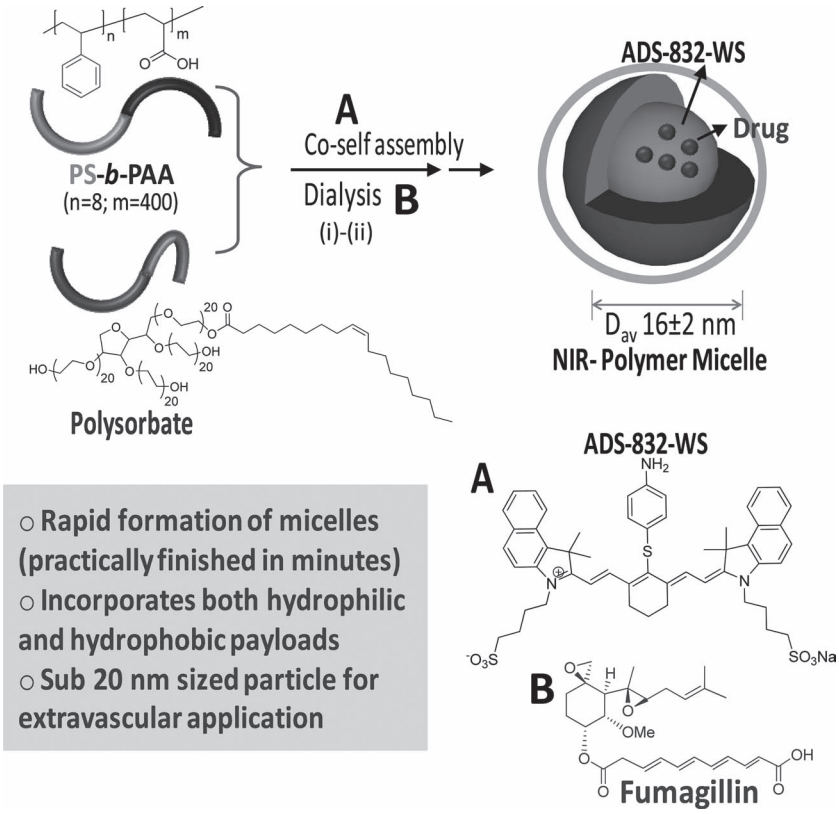

Scheme 1. Synthesis and characterization of theranostic polymeric micelles: i) co-self assembly of amphiphilic diblock copolymer and sorbitan monooleate, ADS-832-WS (A) and/or fumagillin (B), sonication, 25 °C, 1 min; ii) dialysis 10 kDa cellulosic membrane, nanopure water (0.2 μM).

2. Results and Discussion

Our design of the polymeric nanoparticle involved a co-self assembly of an amphiphilic diblock copolymer and Polyoxyethylene (20) sorbitan monooleate in water. (**Scheme 1**) Sorbitan monooleate was deliberately chosen as a co-surfactant to impart stability to the micelles and to restrict the particle diameter within 20 nm with low polydispersity. The amphiphilic polymer was PS_8-*b*-PAA_{400} (Mn×10^3, 0.8-*b*-33.0, polydispersity index: PDI = 1.18, 0.00033 mmol, 0.5 mole%).[25] A simple, "one pot" procedure was followed to incorporate a water-soluble near infrared dye (ADS832WS, λ_{ex} = 824 nm, 1.90 × 10^5 L mol^{-1} cm^{-1}) as a surrogate photoacoustic payload, which was facilitated by the use of a co-surfactant. A facile synthetic route was followed, which involved bath sonication at 50 °C to prepare the polymeric micelles. In a typical procedure, PS-*b*-PAA (6 mg) was weighed in a long neck test tube and to this polysorbate (1 mL) and ADS832WS (1 mg) were added. To this mixture, nano pure water (5 ml, 0.2 μm) was added. The mixture was then placed in a preheated bath, protected from light, and sonicated at

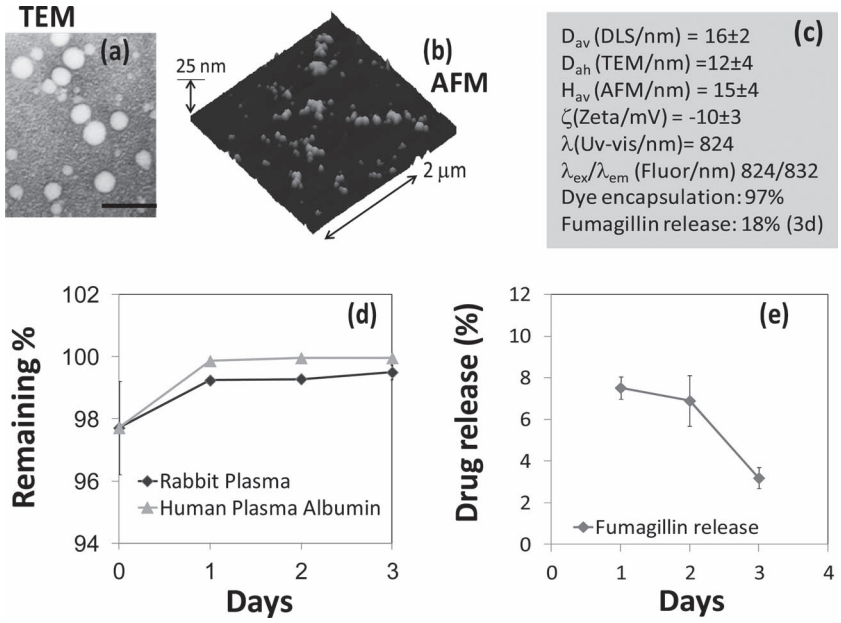

Figure 1. a) TEM image of the polymeric micelles drop deposited over nickel grid, scale bar = 100 nm; b) AFM image of the micelles drop deposited over glass; c) physico-chemical characterization table for a NIR-polymer micelle; d) dissolution of ADS-832-WS from micelle when incubated against rabbit plasma and human plasma albumin; (e) time-dependent release of fumagillin from micelle.

ambient temperature. The mixture turned transparent within 2 min then the particle suspension was dialyzed against infinite sink of nanopure water to remove unbound dye. Ultrasonic bath technique produced a heterogeneous mixture of irregular-shaped micelles as evidenced in the anhydrous state with transmission electron microscopy (TEM). (**Figure 1**a) These morphologies reflected, at least in part, drying artifacts due to the "soft" compliant nature of the particles. However, the difference in hydrophobic chain length between the amphiphilic polymer and the polysorbate may have also contributed to the variable micellar conformations.

Multiple analytical techniques were employed to thoroughly characterize these particles. Dynamic light scattering (DLS) measurements revealed the number-averaged hydrodynamic particle diameter (D_{av}) as 16 ± 2 nm with polydispersitiy (0.021). Electrophoretic potential values ($\zeta = -10 \pm 2$ mV) were measured as negative, which confirmed that the surface was predominantly occupied by the carboxylic acid groups of the hydrophilic segment of the block copolymer. The anhydrous state particle diameter (D_{ah} = 12 ± 04 nm) was calculated from TEM based on a measurement of approx. 100 particles. The discrepancy observed in diameters from hydrated state (DLS) and anhydrous state measurements is presumably due to the flattening of the polymers on the TEM surface. Atomic force microscopy (AFM) in anhydrous state revealed a particle height of 15 ± 04 nm. (Figure 1b) UV-Vis spectroscopy and fluorescence spectroscopy (λ_{ex} = 824 nm; λ_{em} = 832 nm) confirmed the absorbencies at 750–860 nm, corresponding to the presence of the hydrophilic NIR dye. These nanoparticles possess long shelf-life stability (40 days at room temperature).

The synthetic compatibility of this polymeric particle with a hydrophobic therapeutic agent was evaluated using fumagillin, an antiangiogenic drug.[26] A similar protocol was followed as above for the incorporation of the drug, which is highly lipophilic. The precursor agents i.e., amphiphilic diblock copolymer and Polyoxyethylene (20) sorbitan monooleate were co-self assembled in water and the dye was replaced with fumagillin (1 mg). Fumagillin is known to degrade on exposure to intense (carbon arc, high in UV) and even under room light, both in solution and as the solid, with UV absorbance decreasing with a half-life of about 12 hours in solution.[27] Extra precaution was taken to protect the drug and drug loaded particles from light. The sample was preserved in amber vials under dark. Dissolution studies were performed to measure the drug-retentive qualities of the particles. The release of the drug was monitored by UV spectroscopy at λ = 351 nm. Only ~8% releases was observed after day one followed by a release of 7% and 3% respectively after two and three days. A loading efficiency of approximately 97% was determined with excellent retention during dissolution over 4 days in rabbit plasma or against human plasma albumin at 37 °C. (Figure 1d) The release of the dye was monitored by UV spectroscopy at λ = 824 nm. (Figure 1e)

Optoacoustic or photoacoustic tomographic (PAT) imaging is a hybrid, noninvasive, nonionizing modality, which uniquely marries conventional ultrasound and optical imaging. A laser pulse is transmitted and absorbed by a biological tissue, a nonradiative de-excitation of the absorbed optical energy occurs with a resultant slight increase in temperature due to the thermo-elastic expansion. Both endogenous (e.g. haemoglobin) and exogenous (optical absorbers e.g. gold nanoparticle, indocyanine green) contrast agents have been used in combination with PAT.[10–15] One of the major advantages of PAT over the conventional optical imaging is its ability to image deep vasculature. Wang and co-workers have previously demonstrated that optimized PAT could be used to image objects embedded at depths of as much as 5.2 cm, 6.2 times the 1/e optical penetration depth, in chicken breast muscle at a resolution of <780 μm and a sensitivity of <7 pmol of indocyanine green (ICG) in blood.[12b] These results suggest that nonionizing PAT can potentially image deep vasculatures in the breast and other organs.

PAT was used to assess the baseline detection of the NIR-doped polymer particles in rat whole blood. **Figure 2**a shows the PA signals obtained from a tygon tube (I. D. 250 μm, O. D. 500 μm) filled with NIR-polymer nanoparticle and whole rat blood. The laser was tuned to 750 nm. At this excitation wavelength, the peak-to-peak PA signal amplitude obtained from polymer nanoparticle was 320 mV, compared to 130 mV peak-to-peak PA signal amplitude from blood alone. Figure 2b shows the PA spectrum (peak-to-peak PA signal amplitude

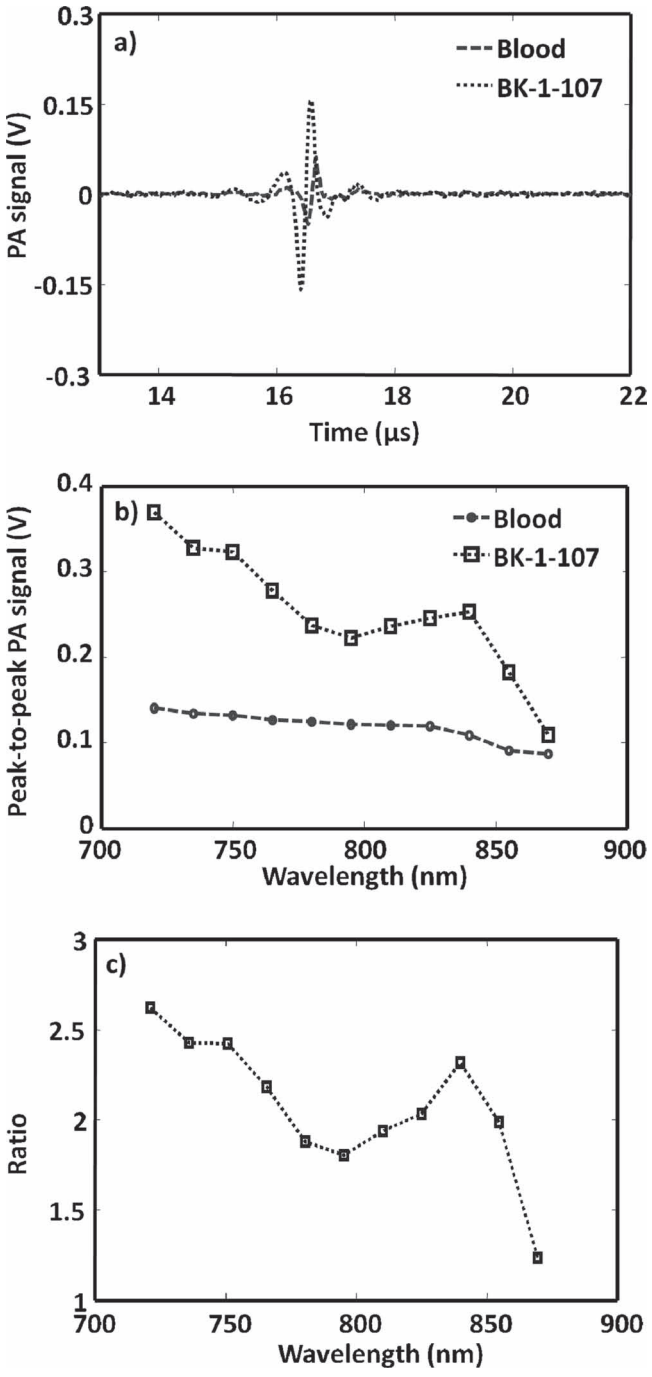

Figure 2. PA imaging of NIR polymer nanoparticle against blood. a) PA spectroscopy signals generated from a tygon tube (I. D. 250 μm, O. D. 500 μm) filled with NIR-polymer micelle and rat blood. The laser was tuned to 750 nm wavelength. b) PA spectrum of NIR-polymer micelle and rat blood over a 720–870 nm NIR wavelength range. c) Ratio of the peak-to-peak PA signal amplitudes generated from polymeric nanoparticle to those of blood.

versus excitation light wavelength) of the NIR-polymer nanoparticle (in blue) for an excitation wavelength range of 720–870 nm. The PA spectrum of rat blood (in red) is also shown in the same figure. These results show that the PA signal obtained from polymer nanoparticle exceeded the inherent blood signal over the NIR entire bandwidth studied. Figure 2c plots the ratio of the peak-to-peak PA signal amplitude of NIR-polymer nanoparticle to that of blood between 720 and 870 nm. This experiment demonstrated that the NIR polymeric nanoparticles generated strong PA signals beyond that of blood, suggesting their utility for *in vivo* imaging.

As previously discussed, the identification of axilliary lymph nodes through real-time PA guidance of sentinel lymph node (SLN) biopsy could decrease resection time by providing precise and accurate spatial localization of the SLN, which is poorly achieved with current optical and nuclear techniques. In the present study, we evaluated the in vivo stability and utility of the polymeric nanoparticles to deliver a NIR dye payload to the sentinel lymph node. **Figure 3**e shows a representative digital photograph of a rat acquired prior to image acquisition with its axillary surface shaved for PA imaging. Before the NIR-polymer nanoparticle injection, a PA control image was obtained, which is shown in the form of a maximum intensity projection (MAP) in Figure 3a. The vasculature near an axial node (one blood vessel is marked as BV) was clearly imaged, with a good resolution of ~500 μm. Note that no lymph nodes were visible in the control image, since the intrinsic optical absorption of lymph nodes was negligible without PA contrast. Following intradermal NIR-polymeric nanoparticle injection, the PA image MAP of the same area immediately (Figure 3b) revealed the lymph node with up to ~510% contrast enhancement which persisted for 30 minutes. Marked but declining contrast enhancement of the draining lymph node was appreciated for 110 minutes. Figures 3c–d are the post-injection PA images (MAP) of the same region 35 min and 110 min after the NIR-polymer nanoparticle injection, respectively. The SLN appears approximately in the center of the images, marked as SLN, and was clearly visible in all of the post-injection PA images (Figures 3b–d). Figure 3f depicted the same rat with the skin removed after the completion of the PA imaging. Figure 3g presents the animal following excision of the SLN (arrow in Figure 3f). Comparing the excised SLN size (3 to 4 mm) with the PA image revealed a close match. (Figures 3b–d).

These polymeric particles were markedly smaller than the gold nanobeacons previously reported for PA sentinel imaging, which was reflected in more rapid particle migration from the paw to the axillary node. (Figure 3h). This exceptionally rapid and persistent (110 min) enhancement of the sentinel lymph nodes with the polymeric NIR particles suggests that flexible, real-time interoperative use rather than the typical perioperative patient procedure may be possible. Such an approach offers greater convenience and reduced procedural expense, as well as improved surgical advantage given the ability to directly and rapidly recognize the depth and orientation of the nodes with intraoperative PAT as the patient is positioned on the table for easier resection. In contradistinction, the current most sensitive techniques with radio-labeled colloids provide only low lateral plane resolution to guide the site of incision but limited vertical resolution to anticipate the depth of dissection required. Interestingly, rather than being permanently entrapped or phagocytosed within the lymph nodes, the tiny NIR particles retained their structural integrity and migrated out into the lymphatic chain and into the circulation via the thoracic duct.

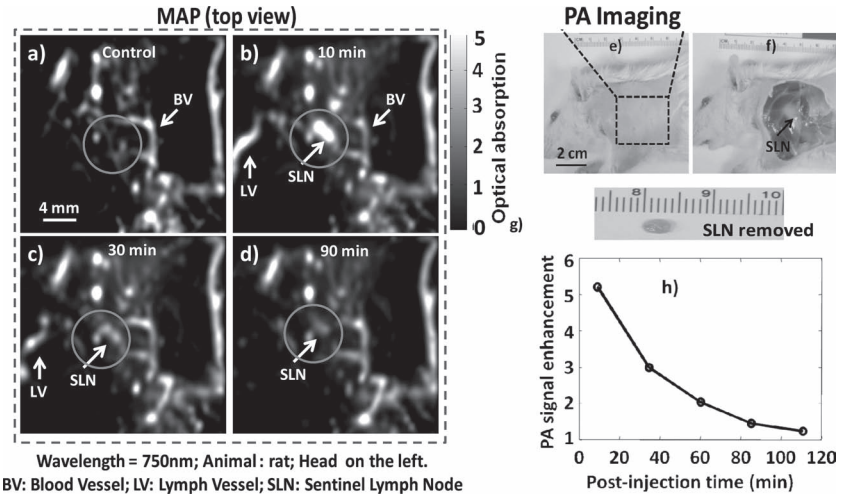

Figure 3. Non-invasive in vivo PA images of SLN in rat: For all PA images, the laser was tuned to 750 nm wavelength. a) Control PA image acquired before polymeric nanoparticle injection. Bright parts represent optical absorption, here, from blood vessels (BV). b) PA image (MAP) acquired immediately after the polymeric nanoparticle injection. c) 35 min post-injection PA image. d) 110 min post-injection PA imageBlood vessel (BV), lymph vessel (LV) and sentinel lymph node (SLN) are marked with arrows, and the SLN is visible in (b)–(d), however, invisible in (a). e) Photograph of the rat after the hair was removed from the scanning region before taking the PA images. The scanning region is marked with a black dotted square. f) Photograph of the rat with the skin removed after PA imaging. g) Excised lymph node. Smallest tick: 1 mm. h) PA signal enhancement in the SLN after the injection of polymeric nanoparticle as a function of post-injection time. For (a)–(d): FOV = 25 mm × 24 mm, step size along the X direction = 0.2 mm, step size along the Y direction = 0.4 mm, total scan time = ~23 min. No signal averaging was used.

Observance of this interesting behavior prompted us to explore and compare the vascular pharmacokinetics and biodistribution of NIR-polymeric nanoparticles injected intravenously and intradermally. A bolus dose (1 ml/kg body weight) was injected I. V. and I. D. and mice were dynamically imaged with IVIS Spectrum NIR optical imaging system (Caliper Life Sciences) every three minutes for thirty minutes. Following I. V. injection, an immediate enhancement of the major blood bearing organs (i.e. heart, spleen, liver, kidney, lymph nodes) was appreciated. (**Figure 4**)

Biodistribution of the polymeric nanoparticles were determined at 24 hours post I. V. and I. D. injection. Animals (n = 3) were sacrificed; major organs were excised and imaged with IVIS. For both the I. D. and I. V. injected animals, the liver was the predominant organ of nanoparticle accumulation as evident from the measured fluorescence intensity. For I. V. injected animals, the other major clearance organs were kidney, lung and lymph node whereas spleen and heart did not produce significant fluorescence signal. Spleen, heart, kidney and liver were the major sites of nanoparticle accumulation for the I. D. injected animal. It is also interesting to note that for the intradermally injected animals, the lymph node accumulation was much higher in comparison to the intravenously injected animal. (**Figure 5**) These data suggest NIR-polymeric nanoparticles presumably follow a typical bio-distribution routes and getting cleared through the reticuloendothelial (RES) system when intravenously delivered. For the intradermally injected particles, more overall fluorescence signal were seen after 24 h, indicating that a slower mechanism of clearance.

3. Conclusions

In conclusion, we report a simple but efficient synthesis of sub-20 nm polymeric nanoparticles incorporating therapeutic or contrast payloads. The use of polysorbate as a co-surfactant during the self assembly process helped to stabilize the tiny micelles and allowed incorporation of both hydrophilic (NIR dye) and hydrophobic (fumagillin) payloads with high encapsulation efficiency (>97%). For PAT imaging of sentinel lymph nodes, the time to lymph node signal was very high and very rapid, which could accommodate rapid, flexible and direct intraoperative use, precluding the need for perioperative procedures and reducing the potential for inadequate or mislabelling. We demonstrate the effectiveness of this theranostic platform for real-time high-resolution intraoperative PA imaging, which may facilitate direct assessment of the sentinel lymph nodes (SLN)

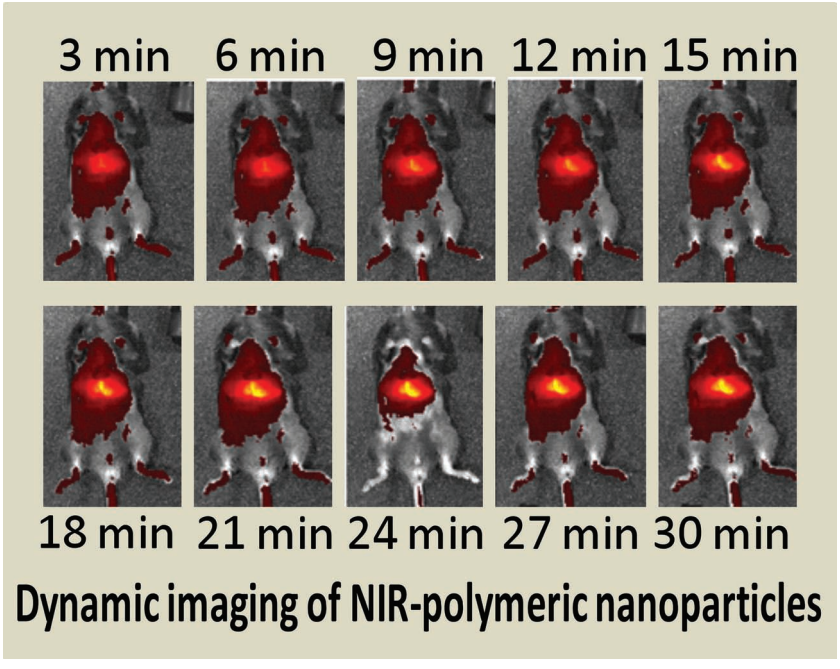

Figure 4. In vivo dynamic fluorescence imaging of IV injected polymeric nanoparticle. Images were acquired using IVIS spectrum (Caliper) at 3 min interval for 30 min.

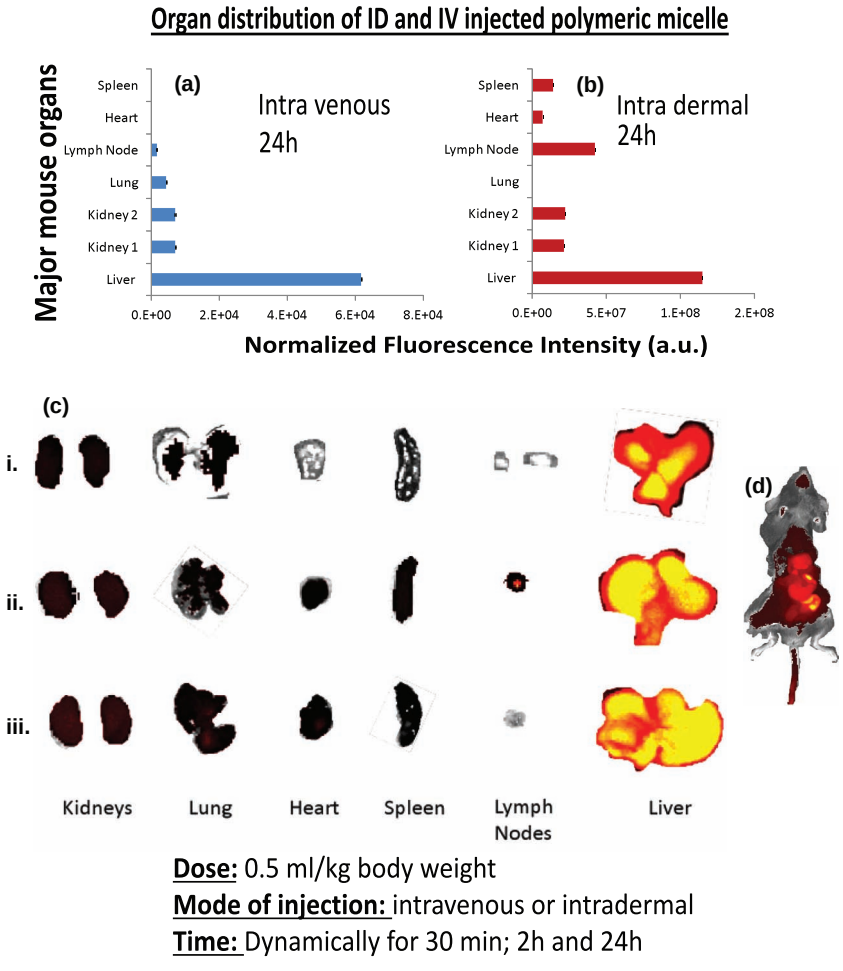

Figure 5. In vivo bio-distribution of NIR-polymeric nanoparticles. Organ distribution of the nanoparticles based on normalized fluorescent intensities in major organs 24 h after a) intravenously and b) intradermally injected particles; c) excised major organs (kidney, lung, heart, spleen, lymph nodes and liver) collected i) 2 h after intravenously injected particles; (ii) 24 h after intradermally and (iii) intravenously injected particles. d) Rodent exposed 2 h after intravenous injection with nanoparticles. [ID: intradermal; IV: intravenous injection]

in breast cancer staging. The technique offers huge potential providing faster resection of SLN and may minimize complications caused by axillary exploration due to mismarking with dyes or low resolution imaging techniques. The biodistribution of polymeric nanoparticles intravenously injected in rodent models were found to follow the anticipated RES pathway. For intradermally injected particles, slower clearance mechanism was observed.

4. Experimental Section

Materials: Unless otherwise listed, all solvents and reagents were purchased from Aldrich Chemical Co. (St. Louis, MO) and used as received. Anhydrous chloroform and methanol were purchased from Aldrich Chemical Co. Poly(styrene-*b*-acrylic acid)[25] (PS-*b*-PAA) was purchased from Polymer Source Inc. (Montreal, Canada). Polyoxyethylene (20) sorbitan monooleate was purchased from Aldrich. Argon and nitrogen (Ultra High Purity: UHP, 99.99%) were used for storage of materials. The Spectra/Por membrane (Cellulose MWCO: 20 000 Da) used for dialysis was obtained from Spectrum Medical Industries, Inc. (Laguna Hills, CA).

Synthesis of Polymeric Micelles: Typical procedure for the preparation of dye-loaded (or drug loaded) polymeric micelles: Polyoxyethylene (20) sorbitan monooleate (Aldrich, Inc., 1 ml, 0.81 mmol) and PS_8-*b*-PAA_{400}[25] ($Mn \times 10^{-3}$: 0.8-*b*-29.3 polydispersity index: PDI = 1.18, 0.00033 mmol, 6.0 mg, 0.5 mole%) were weighed in a long necked tube. The dye ADS832WS (American Dye Source, Inc., 1 mg, absorption coefficient: 1.90×10^5 L mol^{-1} cm^{-1}) was added to this mixture. To this mixture 8 ml of nanopure water (0.2 µm) was added then briefly probe sonicated at ambient temperature for 2 minutes until a transparent suspension was achieved. The dye-loaded particles were transferred into 10,000 Da MWCO cellulose membrane dialysis tubing and dialyzed against water for 2 days with multiple water exchanges. The nanoparticles were recovered, passed through a 0.45 µm Acrodisc Syringe filter into serum vials, sealed under argon, and stored at 4 °C until use. For drug-loaded particles, the same protocol was followed and the dye was replaced with fumagillin (1 mg).

Dynamic Light Scattering Measurements (DLS): Hydrodynamic diameter distribution and distribution averages for the polymeric particles in aqueous solutions were determined by dynamic light scattering. Hydrodynamic diameters were determined using a Brookhaven Instrument Co. (Holtsville, NY) Model Zeta Plus particle size analyzer. Measurements were made following dialysis (MWCO 50 kDa dialysis tubing, Spectrum Laboratories, Rancho Dominguez, CA) of nanoparticle suspensions into deionized water (0.2 µM). Nanoparticles were dialyzed into water prior to analysis. Scattered light was collected at a fixed angle of 90°. A photomultiplier aperture of 400 mm was used, and the incident laser power was adjusted to obtain a photon counting rate between 200 and 300 kcps. Only measurements for which the measured and calculated baselines of the intensity autocorrelation function agreed to within +0.1% were used to calculate nanoparticle hydrodynamic diameter values. All determinations were made in multiples of five consecutive measurements.

Electrophoretic Potential Measurements (Zeta Potential): Zeta potential (ζ) values for the polymeric particles were determined with a Brookhaven Instrument Co. (Holtsville, NY) model Zeta Plus zeta potential analyzer. Measurements were made following dialysis (MWCO 50 kDa dialysis tubing, Spectrum Laboratories, Rancho Dominguez, CA) of nanoparticles suspensions into water. Data were acquired in the phase analysis light scattering (PALS) mode following solution equilibration at 25 °C. Calculation of ζ from the measured nanoparticle electrophoretic mobility (μ) employed the Smoluchowski equation: $\mu = \varepsilon\zeta/\eta$, where ε and η are the dielectric constant and the absolute viscosity of the medium, respectively. Measurements of ζ were reproducible to within ±4 mV of the mean value given by 16 determinations of 10 data accumulations.

Fluorescence Spectroscopy: Fluorescence spectroscopy was performed to confirm the presence of the dye ADS832WS within the nanoparticle. Nanoparticle suspension was excited at (λ_{ex} = 824 nm; λ_{ex} = 832 nm. Fluorescence spectroscopic measurements was made with a Cary Eclipse fluorescence spectrophotometer equipped with Cary Eclipse modular software.

Transmission Electron Microscopy Measurements (TEM): Glow discharged carbon/formvar coated nickel grids were floated on a drop of sample for 2 mins. Grids were blotted, rinsed quickly in water, and

stained in 1% aqueous uranyl acetate (UA) for 1 min. Samples were blotted, air dried, and viewed on a Zeiss 902 Electron Microscope, and recorded with Kodak E. M. film. Micrographs were collected at 100,000× magnification.

Atomic Force Microscopy Measurements (AFM): A Digital Instruments Dimension 3000 series AFM (calibration date 08/2008) and standard Veeco tapping mode silicon probes with platinum-iridium (PtIr) coating were used for scanning the samples. Typically, aqueous suspensions of polymeric samples were dried in a class 10000-clean room on a clean glass slide for 3 h. Once dried, samples were placed on the AFM and scanned. Pertinent scanning parameters were as follows: Resonant frequency (probe): 60-80 kHz; Example of tip velocity: (4 um/s for 2 um), (15 um/s for 5 um), (30 um/s for 10 um). Aspect ratio: 1:1; Resolution: 512 samples/line, 256 lines.

Animal Research Studies: Guidelines on the care and the use of laboratory animals at Washington University in St. Louis were followed for all animal experiments. For sentinel lymph node imaging, adult Sprague Dawley rats (250–350 g) were anesthetized with a mixture of ketamine (85 mg/kg) and xylazine (15 mg/kg) and maintained on 0.75–1.0% isoflurane delivered through a calibrated vaporizer. Polymeric nanoparticles were administered (1 ml/kg) intradermally into the forepaw of the rat. Optical images were acquired before and after the administration of the nanoparticle. During image acquisition, anesthesia was maintained with isoflurane (1 L/min oxygen and 0.75% isoflurane, Euthanex Corp.) and vital signs and pulse oximetry (NONIN Medical INC., 8600 V) was monitored continuously. Hydration was maintained by infusing 8 ml of 0.9% saline subcutaneously into the animal at a distal site as needed. After image acquisition, the animals were euthanized by pentobarbital overdose. For biodistribution studies, polymeric nanoparticles were administered (500 µl total volume) to anesthetized mice (n = 3/route of injection) mice, as described above, by tail vein infusion or intradermal injection. After 24 hours the treated mice were sacrificed with a pentobarbital overdose and their major organs (i.e., liver, spleen, kidney, heart, lung, spleen, lymph node) were excised and imaged *ex vivo* with a Xenogen IVIS Spectrum imaging system.

Optical Imaging System: In vivo fluorescence images were acquired and analyzed with a Xenogen IVIS Spectrum imaging system (Caliper LifeSciences, Hopkinton, MA, USA). During the image acquisition, the mice were maintained under isoflurane inhalation anesthesia. The settings (excitation, 830 nm; emission, 832 nm; exposure time, 0.5 s; binning factor, 8; f value, 2; and field of view, 12.9) were used for imaging acquisitions from the animals intravenously injected with fluorescence-labeled micelles.

Photoacoustic Imaging System: Light source: tunable Ti:sapphire laser (720 nm, LT-2211A, LOTIS TII) pumped by a Q-switched Nd:YAG (LS- 2137/2, LOTIS TII); pulse width <15 ns, pulse repetition rate 10 Hz. The incident laser fluence on the sample surface was controlled to conform to the American National Standards Institute standards. Transducer: 5 MHz central frequency, spherically focused, 2.54 cm focal length; 1.91 cm diameter active area element, 72% bandwidth (V308, Panametrics-NDT); low-noise amplifier (5072PR, Panametrics-NDT). Data were acquired with a digital oscilloscope (TDS 5054, Tektronix).

Acknowledgements

The financial support from the AHA 0835426N, NIH under the Grants NS059302, CA119342, R01 EB000712, R01 EB008085, R01 CA134539, and U54 CA136398 and HL073646 and the NCI under the Grant N01CO37007 is greatly appreciated. L. V. W. has a financial interest in Microphotoacoustic, Inc. and Endra, Inc., which, however, did not support this work. We thank Prof. Samuel A. Wickline for valuable discussion and suggestion on the manuscript.

Received: March 1, 2012
Revised: April 18, 2012
Published online: July 12, 2012

[1] M. S. Kothari, J. E. Rusby, A. A. Agusti, F. A. MacNeill, *Eur J. Surg. Oncol.* **2012**, *38*, 8.
[2] B. Gerber, K. Heintze, J. Stubert, M. Dieterich, S. Hartmann, A. Stachs, T. Reimer, *Breast Cancer Res. Treat.* **2011**, *128*, 613.
[3] B. Cady, M. D. Stone, J. G. Schuler, *Arch. Surg.* **1996**, *131*, 301.
[4] B. G. Haffty, B. Ward, P. Pathare, *J. Clin. Oncol.* **1997**, *15*, 691.
[5] U. Veronesi, G. Paganelli, G. Viale, *N. Engl. J. Med.* **2003**, *349*, 546.
[6] a) D. Krag, D. Weaver, T. Ashikaga, F. Moffat, V. S. Klimberg, C. Shriver, S. Feldman, R. Kusminsky, M. Gadd, J. Kuhn, S. Harlow, P. Beitsch, *N. Eng. J. Med.* **1998**, *339*, 941; b) K. M. McMasters, T. M. Tuttle, D. J. Carlson, C. M. Brown, R. D. Noyes, R. L. Glaser, D. J. Vennekotter, P. S. Turk, P. S. Tate, A. Sardi, P. B. Cerrito, M. J. Edwards, *J. Clin. Oncol.* **2000**, *18*, 2560.
[7] O. A. Ung, *Asian J. Surg.* **2004**, *27*, 284.
[8] A. D. Purushotham, S. Upponi, M. B. Klevesath, L. Bobrow, K. Millar, J. P. Myles, S. W. Duffy, *J. Clin. Oncol.* **2005**, *23*, 4312.
[9] D. N. Krag, S. J. Anderson, T. B. Julian, A. M. Brown, S. P. Harlow, J. P. Costantino, T. Ashikaga, D. L. Weaver, E. P. Mamounas, L. M. Jalovec, T. G. Frazier, R. D. Noyes, A. Robidoux, H. M. C. Scarth, N. Wolmark, *Lancet Oncol.* **2010**, *11*, 927.
[10] X. D. Wang, Y. J. Pang, G. Ku, X. Y. Xie, G. Stoica, L. H. V. Wang, *Nat. Biotechnol.* **2003**, *21*, 803.
[11] X. D. Wang, X. Y. Xie, G. Ku, L. H. V. Wang, *J. Biomed. Opt.* **2006**, *11*, 024015.
[12] a) M. L. Li, J. T. Oh, X. Y. Xie, G. Ku, W. Wang, C. Li, G. Lungu, G. Stoica, L. H. V. Wang, *Proc. IEEE* **2008**, *96*, 481; b) G. Ku, L. H. V. Wang, *Opt. Lett.* **2005**, *30*, 507.
[13] a) A. Agarwal, S. W. Huang, M. O'Donnell, K. C. Day, M. Day, N. Kotov, S. Ashkenazi, *J. Appl. Phys.* **2007**, *102*, 064701–4; b) A. D. Zerda, C. Zavaleta, S. Keren, S. Vaithilingam, S. Bodapati, Z. Liu, J. Levi, B. R. Smith, T-J. Ma, O. Oralkan, Z. Cheng, X. Chen, H. Dai, B. T. Khuri-Yakub, S. S. Gambhir, *Nat. Nanotechnol.* **2008**, *3*, 557.
[14] M. Pramanik, K. H. Song, M. Swierczewska, D. Green, B. Sitharaman, L. H. V. Wang, *Phys. Med. Biol.* **2009**, *54*, 3291.
[15] a) D. Pan, P. Pramanik, A. Senpan, X. Yang, K. H. Song, M. S. Scott, H. Zhang, P. J. Gaffney, S. A. Wickline, L. V. Wang, G. M. Lanza, *Angew. Chem.Int. Ed.* **2009**, *48*, 4170; b) D. Pan, M. Pramanik, A. Senpan, S. Ghosh, S. A. Wickline, L. V. Wang, G. M. Lanza, *Biomaterials* **2010**, *31*, 4088.
[16] a) K. H. Song, E. W. Stein, J. A. Margenthaler, L. H. V. Wang, *J. Biomed. Opt.* **2008**, *13*, 054033; b) M. Pramanik, K. H. Song, M. Swierczewska, D. Green, B. Sitharaman, L. H. V. Wang, *Phys. Med. Biol.* **2009**, *54*, 3291; c) K. H. Song, C. Kim, K. Maslov, L. H. V. Wang, *Eur. J. Radiol.* **2009**, *70*, 227.
[17] C. Allen, Y. Yu, A. Eisenberg, D. Maysinger, *Biochim. Biophys. Acta.* **1999**, *1421*, 32.
[18] C. J. Hawker, K. L. Wooley, *Science* **2005**, *309*, 1200.
[19] R. K. O'Reilly, C. J. Hawker, K. L. Wooley, *Chem Soc Rev.* **2006**, *35*, 1068.
[20] Z. H. Si, G. C. Wang, H. X. Li, J. L. Yuan, B. L. He, *Chin. Chem. Lett.* **2003**, *14*, 39.
[21] D. Pan, J. L. Turner, K. L. Wooley, *Chem. Commun.* **2003**, 2400.
[22] R. Rossin, D. Pan, K. Qi, J. L. Turner, X. Sun, K. L. Wooley, M. J. Welch, *J. Nucl. Med.* **2005**, *46*, 1210.
[23] D. Pan, J. L. Turner, K. L. Wooley, *Macromolecules* **2004**, *37*, 7109.
[24] W. Zhang, X. Jiang, Z. He, D. Xiong, P. Zheng, Y. An, L. Shi, *Polymer* **2006**, *47*, 8203.
[25] a) G. Laruelle, J. François, L. Billon, *Macromol. Rapid Commun.* **2004**, *25*, 1839; b) H. Huang, T. Kowalewski, E. E. Remsen,

R. Gertzmann, K. L. Wooley, *J. Am. Chem. Soc.* **1997**, *119*, 11653; c) J. Wu, A. Eisenberg, *J. Am. Chem. Soc.* **2006**, *128*, 2880; d) J. Xu, G. Sun, R. Rossin, A. Hagooly, Z. Li, K. I. Fukukawa, B. W. Messmore, D. A. Moore, M. J. Welch, C. J. Hawker, K. L. Wooley, *Macromolecules* **2007**, *40*, 2971; e) A. Avital, E. Shapiro, V. Doviner, Y. Sherman, S. Margel, M. Tsuberi, C. Springer, *Am. J. Respir. Cell Mol. Biol.* **2002**, *27*, 511.

[26] N. Sin, L. Meng, Mq. Wang, J. J. Wen, W. G. Bornmann, C. M. Crews, *Proc. Natl. Acad. Sci. U.S.A* **1997**, *94*, 6099.

[27] J. Kochansky, M. Nasr, *Apidologie* **2004**, *35*, 301.